Phys. Status Solidi B **248**, No. 10, 2389–2397 (2011) / **DOI** 10.1002/pssb.201147096

physica status solidi b
www.pss-b.com
basic solid state physics

Feature Article

Non-linear magnetoelastic coupling in monolayers: Experimental challenges and theoretical insights

Dirk Sander* **and Jürgen Kirschner**

Max-Planck-Institute of Microstructure Physics, Weinberg 2, 06120 Halle, Germany

Received 22 February 2011, revised 22 March 2011, accepted 25 March 2011
Published online 18 April 2011

Dedicated to Manfred Fähnle on the occasion of his 60th birthday

Keywords magnetic anisotropy, magnetoelastic coupling, magnetostriction, nanostructures, stress, thin films

* Corresponding author: e-mail sander@mpi-halle.de, Phone: +49 345 5582 660, Fax: +49 345 5511 223

Recent results of experimental studies on magnetoelastic coupling in epitaxial monolayers are compiled and discussed in view of theoretical work. The observation of non-bulk like magnetoelastic coupling in strained systems in experiment and theory is ascribed to an effective and strain-dependent magnetoelastic coupling. It is described as a second-order strain contribution to the energy density. We comment on the importance of inhomogeneous strain and of its relaxation for the magnetic anisotropy of nanostructures.

1 Introduction The magnetic properties of atomic layers and nanostructures often deviate sharply from that of their bulk counterparts. A most intriguing aspect is a change of the easy magnetization direction [1]. The easy magnetization direction of a crystalline bulk sample is along a distinct crystallographic direction, which differs for various elements. The spin–orbit interaction of the electrons gives rise to the so-called magnetocrystalline anisotropy, and it is responsible for the easy magnetization direction of bulk Fe along [100], whereas, for Ni it is along [111] [2]. However, the easy magnetization direction of Fe or Ni *monolayers* can be tuned by the preparation conditions. Monolayers of Fe may exhibit an easy magnetization direction [110], and those of Ni along [100]. Substrate, film thickness, film morphology, adsorbate coverage, and temperature have been identified as decisive factors which determine the easy magnetization direction [1, 3–7]. This possibility to tune the magnetic anisotropy of magnetic layers is the basis for their successful integration in a multi-billion Euro economy dealing with products such as sensors and data storage [8].

But how is this possible? What is the electronic origin of the correlation between magnetic anisotropy and the aforementioned experimental parameters? The quest for answering these highly relevant and demanding questions has triggered fundamental research activities in experiment *and* theory. These studies have established that a decisive factor which determines the magnetic anisotropy of a magnetic layer is its lattice strain. Manfred Fähnle's work on magnetoelastic effects has provided significant and novel contributions to a deeper understanding of the electronic origin of the coupling between strain and magnetic anisotropy in ultrathin films [9–15], and we refer to it repeatedly. One of Fähnle's important contributions is the consideration of strain-dependent magnetoelastic coupling coefficients. *Ab initio* based calculations led him and his coworkers to the insight that contributions to the energy density of first and second order in strain need to be considered.

In the following we highlight selected aspects of our experimental work on magnetoelastic coupling in epitaxial films with regard to Fähnle's work on second-order magnetoelastic effects. The inclusion of second-order effects in magnetoelasticity is one of the most significant results of recent research on this topic. It clearly highlights that lattice strain induces a variation of the magnetoelastic properties, where magnitude and sign of the respective magnetoelastic coupling constants B_i deviate from the respective bulk values. Both experiment and theory support this result. Note that due to the significant magnitude of B_i (several MJ m^{-3}, several 100 μeV/atom) already a small

lattice strain ε in the sub-percent range renders the magnetoelastic anisotropy contribution of order $B \times \varepsilon$ a significant, often the most relevant contribution to the magnetic anisotropy [1, 6, 16].

We start with a brief remark on the relation between magnetoelastic coupling and magnetostriction in Section 2, where we point out distinct differences between the two for the application to film–substrate composites as compared to bulk samples. A brief sketch of the experimental determination of magnetoelastic effects in epitaxial monolayers follows in Section 3. We discuss selected results of magnetoelastic coupling of epitaxial layers in view of theoretical work in Section 4. We conclude with an outlook on the impact of strain relaxation near the border of a nanostructure on the resulting magnetic anisotropy in Section 5.

2 Magnetoelastic coupling and magnetostriction A link between lattice strain and magnetization has been discovered already some 170 years ago by J. P. Joule [17, 18]. Joule measured the tiny extension of steel bars upon magnetization with the help of a mechanical lever device, and also with an optical microscope. He found that the magnetization of an Fe wire along its length leads to a strain along the length of 1.4×10^{-6} (of order ppm). Even from today's perspective the measurement of such a tiny strain is a challenge, and it remains a brilliant success of Joule's experiments to identify this effect. Today, we may look at this experiment as the first measurement of *magnetostriction*, i.e., the change of length of a sample upon magnetization.

Kittel offers a description of the underlying physics in a phenomenological approach of various contributions to the energy density of a magnetic sample. He derives a link between magnetostriction and magnetic anisotropy [2]. Following Kittel we may say that magnetostriction of Fe occurs because a deviation from its cubic crystalline structure leads to a lower energy. This is ascribed to the strain-dependence of the magnetic anisotropy energy. The strain derivative of the magnetic anisotropy is described by magnetoelastic coupling coefficients B_i, which are also known as magnetoelastic stress. Magnetostriction λ is the lattice strain at which magnetoelastic stress is balanced by the elastic stress resulting from the magnetostrictive strain. A derivation of the respective expressions of the relations between λ and B_i is given in review articles [2, 6].

Magnetostriction λ and magnetoelastic stress B_i are illustrated in Fig. 1. Magnetostriction is a consequence of magnetoelastic coupling, and it is defined for free samples. Our interest is the study of magnetic layers, deposited on a substrate. Here, the magnetic film develops magnetoelastic stress, and the film–substrate composite curves, as indicated in Fig. 1b. The magnetoelastic stress B_i is determined from the stress-induced substrate curvature $1/R$ [19, 20]. Thus, for the discussion of magnetoelastic effects in films the concept of magnetoelastic coupling is most appropriate, and it is applied in both theory and experiment.

In calculations, the dependence of the magnetic anisotropy energy E_{ma} on strain is derived, and the magnetoelastic coupling B_i is extracted from plots of E_{ma} as a function of strain [11, 21, 22]. In experiments, B_i is extracted from the change of curvature of the film–substrate composite upon a reorientation of magnetization, as indicated in Fig. 1b and outlined below in Section 3. Thus, a direct comparison between theory and experiment on the magnitude of B_i is feasible, and we discuss the results in Section 4.

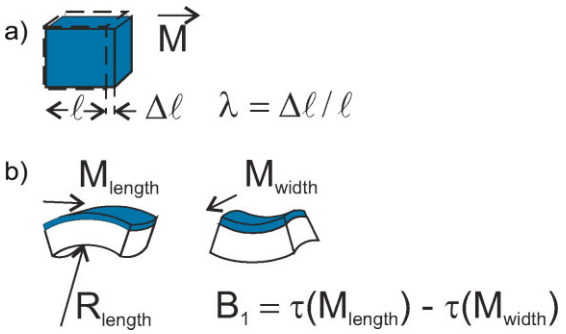

Figure 1 (online color at: www.pss-b.com) Schematic of magnetostriction of a bulk sample (a) and magnetoelastic stress of a film–substrate composite (b). An in-plane reorientation of the magnetization from [100] to [010] of a cubic film induces a curvature change along the sample length, which is proportional to the magnetoelastic coupling coefficient B_1.

Our interest in magnetoelastic effects is also based on its importance for the magnetic anisotropy of strained systems. The magnetoelastic anisotropy contribution of order $B \times \varepsilon$ is a significant, often the most relevant contribution to the magnetic anisotropy [6, 1]. This might come as a surprise in view of the small magnitude of magnetostriction of order 20 ppm in bulk Fe.

Magnetostriction is not necessarily a small effect. FeTb alloys may show magnetostrictive strains of up to 600 ppm, 30 times more than bulk Fe, and this has triggered interest in the application as actuators [23, 24]. Numerous studies have been devoted to FeTb alloys with large magnetostriction. Often, amorphous films are produced, and the impact of internal stress [25] and thermal annealing [26–29] on the magnetistrictive properties has been investigated.

In contrast to magnetoelastic coupling, the concept of magnetostriction involves, among further assumptions on the magnetic reference state, the inclusion of the elastic properties of the sample [2, 6]. Thus, a large magnetostriction might be induced by a low magnitude of the relevant elastic constants c_{ij}.

This aspect is of relevance also in view of recent work on bulk FeGa alloys, where large magnetostriction of 350 ppm, has been reported, and the intriguing interplay between elastic and magnetoelastic properties has been discussed [30]. A description in terms of magnetoelastic coupling avoids this ambiguity, and we focus on magnetoelastic coupling coefficients B_i in the following.

For the theoretical treatment of alloys, such as FeGa, complications due to the potential formation of different structural, compositional, and magnetic phases are expected

[31–35]. Under theses conditions, a change of phase composition will also influence the effective magnetoelastic response of the system, and several, material science related issues contribute to the effect. These effects lead to a most demanding description of magnetoelasticity of alloys., an we focus on single element samples in the following.

3 Experimental aspects The goal of our experiment is to investigate the correlation between lattice strain and magnetoleasticity in epitaxial monolayers. To this end we measure film stress during film growth, and magnetoelastic stress during magnetization reversal *in situ* [6, 36–40]. The former gives us access to lattice strain, and the latter to magnetoelastic coupling. Thus, our data analysis reveals directly how lattice strain influences magnetoelasticity.

The use of stress measurements to extract lattice strain is very powerful, as it gives access to the average film strain in a deposited film [1, 41]. The elastic anisotropy is considered to establish the proper link between stress, and strain in epitaxial samples. The validity of this approach is verified in combined stress and structural determinations by diffraction experiments, such as low energy electron diffraction (LEED) [3, 42] and surface X-ray diffraction (SXRD) [43, 44].

We exploit the stress-induced curvature of a sample to extract film stress during film growth and magnetization reversal [6, 36, 37, 45]. We developed a two-level ultrahigh vacuum (UHV) system as shown schematically in Fig. 2a. Sample preparation, including stress measurements during film growth, is performed on the upper level, and the magnetic characterization by magneto-optical Kerr effect (MOKE) and magnetoelastic stress measurements is done on the lower level. Figure 2b indicates the basis of our optical deflection technique, which is mounted on the upper and lower level for films stress and magnetoelastic stress measurements, respectively. The basic idea is to extract the stress-induced curvature $1/R$ of the sample from an optical two beam deflection measurement, where two laser beams are directed at the sample with a separation of order $\Delta\ell = 4$ mm. Any change of curvature of the sample is measured from the difference of the signals at the upper and lower position sensitive detector. This measurement gives access to the curvature directly. We use samples with a large length ℓ to width w ratio, $\ell/w > 4$, to minimize any issues with regard to clamping effects on the dimensionality of the sample curvature [19]. Typically, the single crystalline metal substrates are $\ell = 12$ mm long, $w = 2.5$ mm wide, and $t_s = 0.1$ mm thin. The optical deflection set up is mounted outside of the UHV chamber at window flanges some $L = 300$ mm away from the sample.

We use the combination of two electromagnets in the bottom part of the UHV chamber, see Fig. 2a, to produce a magnetization of either along the horizontal or vertical direction. We reach fields of order 0.4 and 0.1 T, respectively. The change of the magnetization direction is measured by MOKE [46], and the corresponding magnetoelastic stress change is simultaneously monitored. The measurement procedure is indicated in Fig. 3 for 8 ML Fe on an Ir(100)

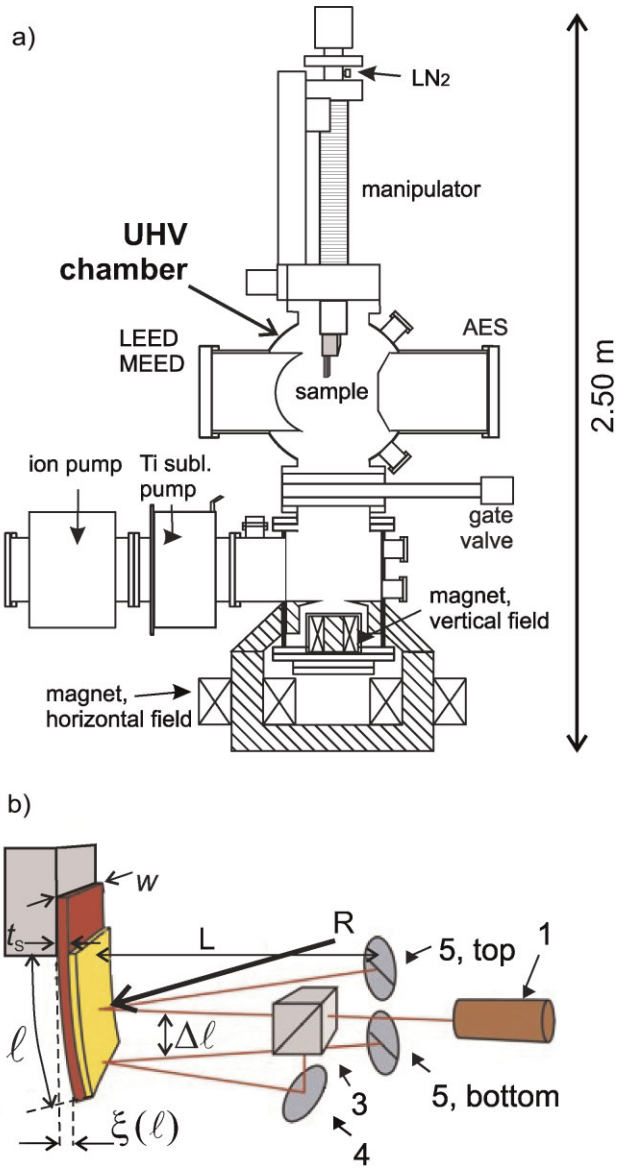

Figure 2 (online color at: www.pss-b.com) (a) Sketch of the UHV chamber for *in situ* stress and magnetic studies. The sample can be lowered with the manipulator from the upper preparation level (LEED, MEED, and AES) to the lower magnet level. At both levels optical deflection measurements as shown in (b) are mounted for stress during growth and magnetization-induced stress measurements, respectively. (b) Optical two beam deflection technique. The substrate of length $\ell(\approx 12$ mm), width $w(\approx 2.5$ mm), and thickness $t_s(\approx 0.1$ mm) is fixed along its width at the top end. The curvature $1/R$ of the substrate is monitored by reflecting two laser beams onto position sensitive detectors. 1, laser; 3, beam splitter; 4, mirror; and 5, position sensitive detector (split-photodiode). See Refs. [36, 37] for further details.

substrate. The plot reveals that upon an reorientation of the film magnetization from along the length to along the width of the sample a magnetoelastic stress change of order 0.01 N/m arises. We conclude that this 8 ML Fe film develops a compressive magnetoelastic stress along the

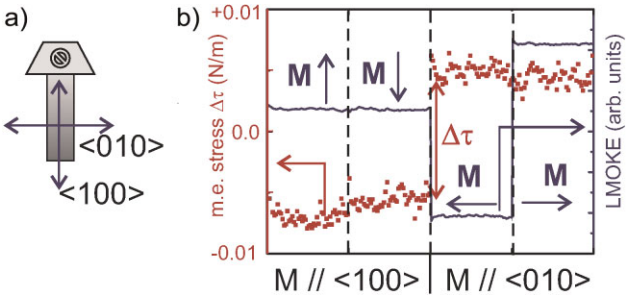

Figure 3 (online color at: www.pss-b.com) Sketch of the magnetization directions (a) for the magnetoelastic stress measurement of 8 ML Fe on Ir(100) at 300 K (b). The red curve shows the magnetoelastic stress change upon a magnetization reorientation in-plane (indicated in (a)), which is monitored also by longitudinal MOKE measurements (LMOKE, blue curve).

magnetization direction, i.e., it has a tendency to expand along the magnetization direction. The quantitative analysis reveals a magnetoelastic coupling coefficient of $B_1 = -10\,\mathrm{MJ\,m^{-3}}$, which is roughly three-times as large as the respective bulk value. As outlined below, we ascribe this to the impact of lattice strain on the magnetoelastic coupling.

To provide an appreciation for the magnitude of the effects we note that the experimental results of Fig. 3 correspond to a sample deflections of several Å and $R \approx 100\,\mathrm{km}$. These are tiny effects, yet they are reliably extracted. Typically, lattice strain induced film stress gives rise to 2–3 orders of magnitude larger deflections and curvatures. The film thickness integrated epitaxial misfit stress of the 8 ML Fe film of Fig. 3 is measured as −9 N/m [47], almost three magnitudes larger than the magnetoelastic stress (0.01 N/m) of the same film.

In the following presentation of the experimental results, we exploit both the measurements of film stress during film growth and the magnetoelastic stress results to present our data on the magnetoelastic coupling as a function of lattice strain.

4 Results: Experimental values as compared to theory Our measurements of film stress and magnetoelastic stress enable us to investigate the relation between film strain and magnetoelastic coupling directly. To this end we have measured for numerous epitaxial systems the magnetoelastic stress for films of different thickness in the low nanometer range. For each film we have also determined the film stress, from which we extract the average film strain. The results of our studies are compiled in Fig. 4 where the respective value B_i is given with respect to the average in-plane film strain. Depending on the epitaxial order and the magnetization direction different coupling coefficients B_i have been determined. A special situation arises for Fe /Cu(001). Here, epitaxial growth leads to the formation of differently oriented bcc Fe (110) crystallites, and the effective magnetoelastic coupling is a function of B_1 and B_2 [41]. On all plots we indicated the respective bulk value of B_i for comparison.

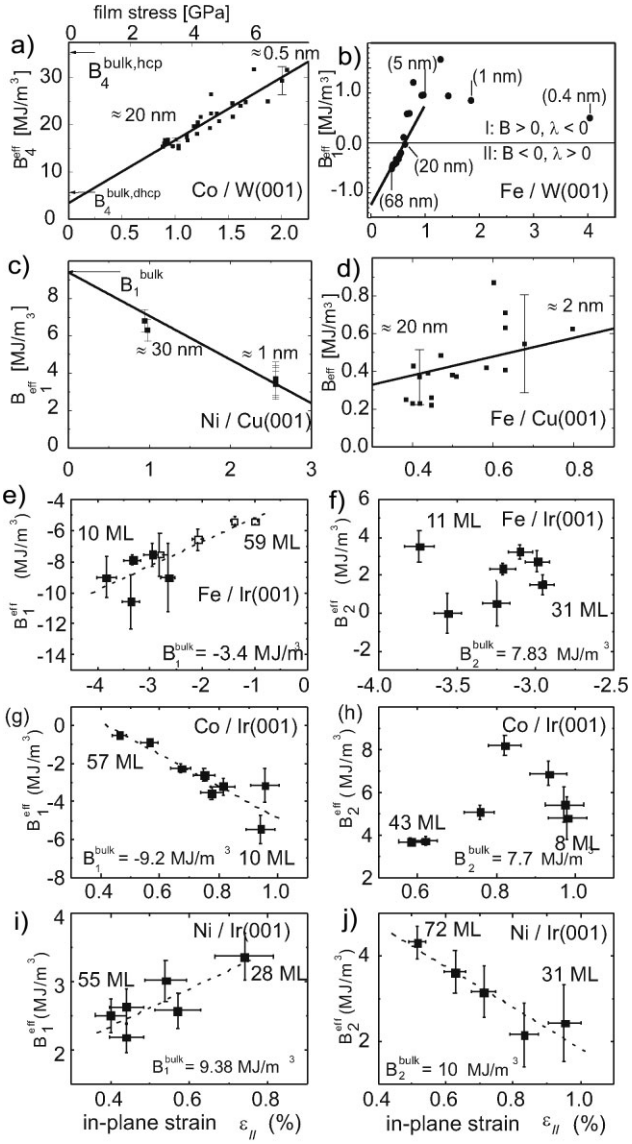

Figure 4 Compilation of experimental results of the effective magnetoelastic coupling B_i as a function of lattice strain for different systems [6, 38, 41, 47]. The respective bulk value is indicated for reference. Note that in (d) the effective B depends on B_1 and B_2 [41].

The most striking result of all measurements is that we find in each case a significant deviation from the bulk value of B_i. The immediate consequence for the discussion of strain-induced magnetic anisotropy is profound: bulk values are *not* the appropriate reference for magnetoelastic coupling in strained epitaxial films.

Close inspection of the results of Fig. 4 reveals, that a linear relation between magnetoelastic coupling and strain gives a reasonable description of the results of Fig. 4a, c–e, g, i, and j. Such a linear relation is valid for Fig. 4b only in a limited strain range 0.5–1%. The scatter of data Fig. 4f and h discourages its description by a linear relation.

What is the physical origin of this non-bulk like behavior? Initially, the deviation of magnetoelastic coupling

from its bulk value has been inferred from surface sensitive measurements of the spin-polarization in artificially strained samples [48, 49]. It has been argued that this might be ascribed to a surface contribution to magnetoelastic coupling. If this was true, than the magnetoelastic coupling should approach bulk properties in the limit of thick films. However, this is at variance with experimental results. Experiments on films with the same thickness but different strain rather suggest that lattice strain is the decisive factor for a deviation of B_i from its bulk value [50, 51]. In the following, we adopt this view [6, 1], which is also corroborated by theoretical results.

In theory, magnetoelastic effects are accessible by *ab initio* density functional calculations of the total energy in a scalar relativistic approach. Spin–orbit interaction, which is the origin of magnetoelastic effects, is treated in a perturbative manner. The exchange correlation functional is treated in the local spin density approximation (LSDA) or with the general gradient approximation (GGA) [11]. A plot of the variation of the total energy of the sample as a function of lattice strain for a change of the magnetization direction is calculated. This plot shows a variation with strain, and it is fitted by a polynomial expression. A linear relation indicates a constant magnetoelastic coupling coefficient, a parabolic relation indicates a second-order strain contribution to the magnetic anisotropy. It can be ascribed to a linear dependence of the magnetoelastic coupling coefficient on lattice strain. High order contributions are feasible, but they are not considered in this approximation [12]. These calculations are challenging and numerically very demanding. To appreciate this we point out that tiny energy variations (magnetoelastic effects) of a large number (total energy) need to be calculated reliably with demanding numerical precision [52].

The compilation of theoretical and experimental results in Table 1 indicates the significant impact of strain on the magnetoelastic coupling. This significance is given by the large magnitude of the factor D_i, which describes the strain dependence of the effective magnetoelastic coupling via $B_i^{\mathrm{eff}} = B_i + D_i\varepsilon$ [47]. Already small strains in the sub-percent range may induce significant deviations of B_i away from its bulk value.

However, Table 1 also reflects significant discrepancies between experiment and theory. Note that different calculational approximations, LSDA as compared to GGA, give different results for the same system. Experimental values for the same element vary for different experiments. The deviations between experiment and theory are thoroughly discussed in Ref. [47]. It has been argued that specific couplings such as B_2 for Fe are notoriously difficult to calculate [13], also the application of a linear strain relation for B_i may be too simplistic. A third-order strain contribution has been suggested for bcc Ni [15]. Further issues concern the difference between experiment and theory on how strain is accounted for in calculations by applying a certain strain state to a bulk sample. The strain state of the calculation generally differs from that of an epitaxially strained film [11, 53]. Also, the finite extension of the film, including interfaces and surfaces relaxation effects, is not considered in calculations.

Irrespective of numerical discrepancies between experiment and theory the results of Table 1 point at the importance of lattice strain for a modified magnetoelastic coupling of strained systems. In the next section we indicate necessary amendments to consider also inhomogeneous strain states which are commonly found at the interface of epitaxial layers and near the borders of laterally confined nanostructures.

5 Strain relaxation at nanostructures and the impact on magnetic anisotropy The present treatment of lattice strain with respect to magnetic anisotropy assumes that lattice strain ε_{ij} is given by lattice misfit and by the

Table 1 Compilation of theoretical values and experimental results of magnetoelastic coupling coefficients B_i and the non-linear strain dependent coefficient D_i with $B^{\mathrm{eff}} = B_i + D_i\varepsilon$ [47]. (All values are given in MJ/m^3).

		B_1	D_1	B_2	$2D_2$	B_4	D_4
fcc Co	LSDA [11, 13]	−15.9	212	3	58		
	GGA [11, 13]	−9.8	186	4.5	−71		
	exp. [6]	−9.2	–	7.7	–		
	Co/Ir(100) [47]	3.5	−842	1.8	930		
fcc Ni	LSDA [11, 13]	12.6	−103	16.9	−132		
	GGA [11, 13]	10.2	−53	11.1	−47		
	Ni/Cu(100) [41]	9.4	−234	10	–		
	Ni/Ir(100) [47]	1.3	273	6.6	−408		
bcc Fe	LSDA [11, 13]	−10.1	337	−7.0	−40		
	GGA [11, 13]	−2.4	383	−3.9	18		
	Fe/MgO(100), Fe/Cr/MgO(100) [51]	−3.4	1100	7.8	−365		
	Fe/Ir(100) [47]	−3.6	155	–	–		
	Fe/W(100) [6]	−1.2	200	–	–		
hcp Co	Co/W(001) [38]					3.4	1346

LSDA, local-spin-density approximation; GGA, generalized-gradient approximation. See Ref. [47] for further remarks and explanations.

epitaxial relation of film growth. For a film thickness beyond pseudomorphic growth, an average lattice strain is considered [1, 38]. In any case, an homogeneous set of strain values is taken to account for the impact on magnetic anisotropy. Local strain relaxations are not accounted for. This approach neglects a common relaxation phenomenon, namely the variation of the layer spacings near the interface of a film–substrate composite [54]. Highly precise structural determinations and corresponding theoretical work have clearly revealed that localized variations of the atomic distances near interfaces are the rule rather than an exception. Well-studied examples include the relaxation of the topmost layer spacing at the vacuum interface. In laterally confined nanostructures, structural relaxations are expected along in-plane and out-of-plane directions and have been studied in experiments and theory [55–58].

Here we present two examples which point at the importance of strain relaxation near interfaces for the magnetic anisotropy. The first example deals with the H-induced spin reorientation transition (SRT) in Ni monolayers [3, 59], where the impact of the H-induced change of vertical layer relaxation is discussed in view of the SRT. The second example deals with nanometer small individual Co islands. Here, the impact of structural relaxation on the resulting magnetic anisotropy has not been discussed yet, but spatially resolved electronic spectroscopy by scanning tunneling microscopy (STM) in combination with theory finds clear evidence for substantial variation of strain on a nanometer length scale [60]. The study of the impact of these three dimensional structural relaxations on the magnetic anisotropy of nanoscale objects remains a challenging task for future work.

5.1 Adsorbate-induced structural relaxation and spin reorientation transition Previous work has established that the reverse SRT in Ni monoalyers on Cu(001) from in-plane to out-of-plane with *increasing* film thickness is intimately linked to the interplay between different contributions to the magnetic anisotropy [59, 61]. The tetragonal distortion of the Ni film favors via the magnetoelastic coupling an out-of-plane easy magnetization direction. However, surprisingly films up to a thickness of 10–11 ML show an in-plane easy magnetization direction, thicker films of up to some 50 ML show an out-of-plane easy magnetization direction. The SRT around 10–11 ML occurs without any structural change of the film, and a variation of the average tetragonal distortion of the film can be excluded as a driving force. Theory suggests that both interfaces, Ni–Cu and Ni-vacuum favor an in-plane magnetization direction. The SRT reflects the change of the resulting magnetic anisotropy, which results from a subtle interplay between volume and interface contributions.

The structure of Ni monolayers on Cu(001) has been studied extensively also by quantitative LEED I(V) measurements before, and these previous studies confirm the pseudomorphic nature of the Ni films in the thickness range of the adsorbate-induced SRT [62, 63].

Table 2 Vertical layer spacings $d_{i,i+1}$ (Å) for the best-fit structures as retrieved by quantitative LEED. The last digit indicates the location of the R-factor minimum with respect to the 0.005 Å structural search grid. Note that the (100) layer spacing in bulk Ni is 1.759 Å. See Ref. [3] for further remarks.

	d_H	d_{12}	d_{23}	d_{34}	d_{45}	d_{56}	d_b
8 ML Ni	–	1.675	1.720	1.705	1.715	1.720	1.710
H/8 ML Ni	0.31	1.770	1.695	1.700	1.710	1.710	1.710

To shed further light on this SRT, we investigated the influence of hydrogen on the SRT. We found that the easy magnetization direction can be switched reversibly from in-plane to out-of-plane in a 8 ML Ni film, by changing the H-partial pressure in the gas phase surrounding the sample at 320 K. A larger H-partial pressure ($p_{H_2} = 2 \times 10^{-8}$ mbar) switches the easy magnetization direction to out-of-plane, whereas, the easy magnetization direction reverts back to in-plane at $p_{H_2} < 2 \times 10^{-9}$ mbar [3].

The important result of our study is summarized in Table 2. We find by quantitative LEED $I(V)$ analysis that the introduction of hydrogen leads to a significantly enlarged layer spacing of Ni at the vacuum interface. Without hydrogen, this distance d_{12} is 1.675 Å, whereas, it expands by almost 0.1–1.77 Å for hydrogen exposure. The second layer spacing shows an opposite trend with much smaller variation of the distances. The inner parts of the films show within error limits the same layer spacing irrespective of H-exposure.

These results provide experimental evidence for the intimate relation between surface relaxation and magnetic anisotropy. They offer new insight into the physical origin of the peculiar magnetic anisotropy of interfaces [64–66]. This phenomenon is a true surface effect, it cannot be ascribed to change of the average vertical lattice strain. The average layer spacing is almost identical for the native and the H-exposed film. This analysis offers an insight into the physical origin of the magnetic surface anisotropy. The significant inward-layer relaxation of the native Ni surface layer appears to be the key factor for its contribution to the magnetic anisotropy.

We conclude that local, spatially confined structural relaxations may have a decisive impact on the magnetic anisotropy of the whole sample. A comprehensive theoretical description must take structural relaxations in the out-of-plane, and for laterally confined samples also in the in-plane directions into account. This aspect is further illustrated in the next section for a nanometer small Co nanostructure.

5.2 Spatial dependence of electronic properties and structural relaxation in individual nanostructures Whereas, the layer relaxation discussed in the previous section is a consequence of the lack of bonding partners *above* the surface, the lack of bonding partners at the rim of a laterally confined sample also induces a corresponding structural relaxation. Theory suggests that

structural relaxations occur in the proximity (few nanometer) of the rim of the nanostructure and at the substrate underneath. These structural relaxations have been evidenced as stress oscillations during layer-by-layer film growth [68, 69], in diffraction studies [56, 58], and also in recent TEM investigations of individual FePt nanostructures [70].

STM and scanning tunneling spectroscopy (STS) allows to study the spatial dependence of electronic properties of an individual nanostructure with high spatial resolution and spin sensitivity [71]. The differential conductance of the tunnel current, and its spatial dependence on an individual nanostructure, is accessible in experiments. This property is linked to the local density of states of the sample at the distance of the tip of the STM above the surface (roughly 4–5 Å). The link between differential conductance and electronic density of states of the sample allows a comparison between STS experiments and theory, as electronic properties of nanostructures are accessible in calculations.

We present in Fig. 5a a measurement of the differential conductance as function of position on a bilayer high nanometer small Co island on Cu(111). The plot reveals a drastic change of the differential conductance with position. The main feature at the center part of the island is a peak around −0.3 V (curves 2 and 3), whereas, near the corner (1) and the rim (4) this feature is strongly reduced, and a new peak at 0 V evolves at the rim.

In conjunction with theory, the peak at −0.3 V is ascribed to a Co-related electronic signature of a minority 3d state [72]. Its peak position has been found to depend sensitively on the structural relaxation of the island [60]. It shifts to more negative values with increasing relaxation toward the island edge. The peak at 0 V is a so-called electronic rim state [73], which is spatially confined to a narrow range of around 1 nm near the island rim. This qualitative inspection highlights the pronounced spatial dependence of electronic properties on the nanoscale. But what is its impact on the magnetism and the magnetic anisotropy of the nanostructure?

This is a most relevant, but also delicate question. To strive for an answer, we performed spin-polarized STM studies to characterize spin-dependent properties with high spatial resolution [67]. We find a pronounced spatial variation of the asymmetry of the differential conductance on an individual Co nanostructure as indicated in Fig. 5b. In conjunction with theory we may infer that the asymmetry map reflects a spatial modulation of the spin-polarization of the Co island [67]. Thus, the results of Fig. 5 may be ascribed to a spatial variation of the spin-dependent electronic properties of an individual nanostructure.

To appreciate these results with respect to the magnetic properties of the whole nanostructure, we need to be aware that STM is sensitive to the electronic properties of the sample measured a few Å above its surface. Also, STM always resembles properties of the tip-sample ensemble [74], and interactions between tip and sample need to be considered [75, 76]. Thus, the link between the spatial variation of spin-dependent STM studies and a possible corresponding spatial variation of magnetic properties such as magnetic moment and magnetic anisotropy is not necessarily trivial. Presently, without further insight from theory, we refrain from a quantitative discussion of spin-polarized STS results in view of magnetic moments and magnetic anisotropy. Nevertheless we stress that a spatial variation of these properties appears very possible based on the variation of the atomic and electronic structure on the nanometer scale.

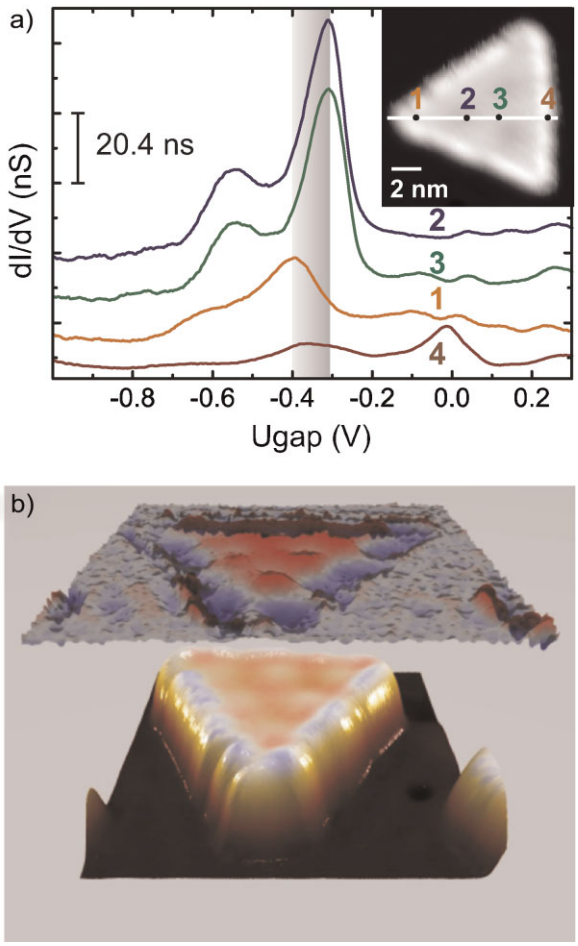

Figure 5 (online color at: www.pss-b.com) (a) Differential conductance d*I*/d*V* measured by STS for different positions 1...4 on a double layer high Co Island on Cu(111). $T = 8$ K. The inset shows a topographic image of the island, where the measurement positions are marked. The d*I*/d*V* signal changes drastically with position. The shift of one peak position is indicated by the gray shaded area. The curves are shifted vertically for clarity. (b) Superposition of a 3D-topographic representation of the bilayer high Co island of (a) with a map of the asymmetry of the differential conductance measured at the Fermi energy. Blue, negative; red, positive; gray, zero asymmetry. The map reflects a spatial modulation of the spin-polarization, induced by spin-dependent electron confinement within the Co island [67]. See text for details.

Summarizing the results of Fig. 5, we conclude that electronic properties vary considerably within a single nanostructure. This may be ascribed to structural relaxation and to spin-dependent electron confinement. These phenomena go far beyond a description in terms of lattice misfit and magnetoelastic coupling, as applied successfully to extended ferromagnetic monolayers above. It appears that the successful treatment of magnetism of individual nanoscale objects needs to consider the corresponding electronic peculiarities explicitly [77]. This renders their theoretical description even more demanding as compared to the already involved treatment of magnetic anisotropy of extended strained layers. More work on this intriguing topic is clearly called for.

6 Conclusions Non-bulk like magnetoelastic coupling in ferromagnetic monolayers has been measured in numerous studies. Experimental results indicate and theory suggests that lattice strain is an important factor for this peculiar magnetoelastic behavior in strained systems. All results corroborate the view that lattice strain itself leads to a change of the respective magnetoelastic coupling coefficients. The effect is pronounced. Magnitude and sign may deviate from the respective bulk values. Thus, higher-order magnetoelastic effects need to be considered. A reliable and profound discussion of the magnetic anisotropy of strained monolayers requires the treatment in view of an effective strain-dependent magnetoelastic coupling. Reference to bulk magnetoelastic coefficients may produce erroneous results.

The agreement between experimental results on the effective magnetoelastic coupling and theoretical predictions is qualitative in some cases, and unsatisfactory in others. It appears to be worthwhile to strive for an improved understanding and description of this fundamental aspect of magnetic anisotropy in an ongoing combined experimental and theoretical effort.

Experimentalist and theorists await further and conceptually new challenges with the present advance of research into the field of magnetic anisotropy of single nanostructures with dozens to thousands of atoms. Here, local strain relaxations are omnipresent, and a non-trivial impact on magnetic anisotropy is expected.

Acknowledgements The authors enjoyed numerous enlightening discussion with Manfred Fähnle on magnetoelasticity and related topics. The experimental work in Halle has been and still is the topic of several Ph.D. theses. Contributions by Axel Enders, Thomas Gutjahr-Löser, Thomas Höpfl, Safia Ouazi, Wei Pan, Zhen Tian, Sebastian Wedekind, Guillemin Rodary, Hirofumi Oka, Anita Dhaka, and Jörg Premper are gratefully acknowledged. The authors enjoyed numerous discussions with Klaus Heinz, Lutz Hammer, Peter Weinberger, Franta Máca, Holger Meyerheim, and Valeri Stepanyuk on structural relaxation at interfaces. We thank Heike Menge for the skillful preparation of thin single crystalline metal substrates. This work was supported by DFG SFB 762.

References

[1] D. Sander, J. Phys.: Condens. Matter **16**, R603–R636 (2004).
[2] C. Kittel, Rev. Mod. Phys. **21**(4), 541–583 (1949).
[3] D. Sander, W. Pan, S. Ouazi, J. Kirschner, W. Meyer, M. Krause, S. Müller, L. Hammer, and K. Heinz, Phys. Rev. Lett. **93**(24), 247203 (2004).
[4] U. Gradmann, Handbook of Magnetic Materials, Vol. 7 (Elsevier Science, Amsterdam, 1993), chap. 1, pp. 1–96.
[5] M. Farle, Rep. Prog. Phys. **61**, 755–826 (1998).
[6] D. Sander, Rep. Prog. Phys. **62**, 809–858 (1999).
[7] C. Klein, R. Ramchal, A. K. Schmid, and M. Farle, Phys. Rev. B **75**(19), 193405 (2007).
[8] P. Grünberg, Phys. Today **54**(5), 31 (2001).
[9] M. Fähnle and M. Komelj, J. Magn. Magn. Mater. **220**, L13–L17 (2000).
[10] M. Komelj and M. Fähnle, J. Magn. Magn. Mater. **220**, L8–L12 (2000).
[11] M. Fähnle, M. Komelj, R. Q. Wu, and G. Y. Guo, Phys. Rev. B **65**(14), 144436 (2002).
[12] M. Fähnle and M. Komelj, Z. Metallkunde/Mater. Res. Adv. Tech. **93**(10), 970–973 (2002).
[13] M. Komelj and M. Fähnle, Phys. Rev. B **65**(9), 092403 (2002).
[14] M. Komelj and M. Fähnle, Phys. Rev. B **65**(21), 212410 (2002).
[15] M. Komelj and M. Fähnle, Phys. Rev. B **73**(1), 012404 (2006).
[16] D. Sander, A. Enders, and J. Kirschner, J. Magn. Magn. Mater. **200**, 439–455 (1999).
[17] J. P. Joule London, Edinburgh Dublin Philos. Mag. J. Sci. **30**, 76–87 (1847).
[18] J. P. Joule London, Edinburgh Dublin Philos. Mag. J. Sci. **30**, 225–241 (1847).
[19] K. Dahmen, H. Ibach, and D. Sander, J. Magn. Magn. Mater. **231**, 74–84 (2001).
[20] P. Farber, M. Hormann, M. Bischoff, and H. Kronmüller, J. Appl. Phys. **85**(11), 7828–7832 (1999).
[21] R. Wu and A. J. Freeman, J. Magn. Magn. Mater. **200**(1–3), 498–514 (1999).
[22] T. Burkert, O. Eriksson, P. James, S. Simak, B. Johansson, and L. Nordström, Phys. Rev. B **69**, 104426 (2004).
[23] E. Quandt, J. Alloys Compd. **258**(1–2), 126–132 (1997), International Conference on Giant-Magnetostrictive.
[24] A. Ludwig and E. Quandt, J. Appl. Phys. **87**(9), 4691–4695 (2000).
[25] F. Schatz, M. Hirscher, M. Schnell, G. Flik, and H. Kronmüller, J. Appl. Phys. **76**(9), 5380–5382 (1994).
[26] K. Ried, M. Schnell, F. Schatz, M. Hirscher, B. Ludescher, W. Sigle, and H. Kronmüller, Phys. Status Solidi A **167**(1), 195–208 (1998).
[27] S. F. Fischer, M. Kelsch, and H. Kronmüller, J. Magn. Magn. Mater. **195**(3), 545–554 (1999).
[28] B. Winzek, M. Hirscher, and H. Kronmüller, J. Alloys Compd. **283**(1–2), 78–82 (1999).
[29] N. H. Duc, T. M. Danh, N. A. Tuan, and J. Teillet, Appl. Phys. Lett. **78**(23), 3648–3650 (2001).
[30] J. Cullen, A. Clark, M. Wun-Fogle, J. Restorff, and T. Lograsso, J. Magn. Magn. Mater. **226–230** (Part 1), 948–949 (2001).
[31] R. Wu, J. Appl. Phys. **91**(10), 7358–7360 (2002).

[32] J. X. Cao, Y. N. Zhang, W. J. Ouyang, and R. Q. Wu, Phys. Rev. B **80**(10), 104414 (2009).
[33] Y. N. Zhang, J. X. Cao, and R. Q. Wu, Appl. Phys. Lett. **96**(6), 062508 (2010).
[34] T. Khmelevska, S. Khmelevskyi, and P. Mohn, J. Appl. Phys. **103**(7), 073911 (2008).
[35] M. Laver, C. Mudivarthi, J. R. Cullen, A. B. Flatau, W. C. Chen, S. M. Watson, and M. Wuttig, Phys. Rev. Lett. **105**(2), 027202 (2010).
[36] D. Sander and J. Kirschner, Appl. Phys. A **87**, 419–425 (2007).
[37] D. Sander, Z. Tian, and J. Kirschner, Sensors **8**, 4466–4486 (2008).
[38] T. Gutjahr-Löser, D. Sander, and J. Kirschner, J. Magn. Magn. Mater. **220**, L1–L7 (2000).
[39] W. Wulfhekel, T. Gutjahr-Löser, F. Zavaliche, D. Sander, and J. Kirschner, Phys. Rev. B **64**, 144422 (2001).
[40] D. Sander, S. Ouazi, A. Enders, T. Gutjahr-Löser, V. Stepanyuk, D. Bazhanov, and J. Kirschner, J. Phys.: Condens. Matter **14**, 4165–4176 (2002).
[41] T. Gutjahr-Löser, D. Sander, and J. Kirschner, J. Appl. Phys. **87**, 5920–5922 (2000).
[42] V. Martin, W. Meyer, C. Giovanardi, L. Hammer, K. Heinz, Z. Tian, D. Sander, and J. Kirschner, Phys. Rev. B **76**, 205418 (2007).
[43] H. Meyerheim, D. Sander, R. Popescu, J. Kirschner, S. Steadman, and P. Ferrer, Phys. Rev. B **64**, 045414 (2001).
[44] H. Meyerheim, D. Sander, R. Popescu, J. Kirschner, O. Robach, S. Ferrer, and P. Steadman, Phys. Rev. B **67**, 155422 (2003).
[45] R. Koch, M. Weber, and K. Rieder, J. Magn. Magn. Mater. **159**, L11–L16 (1996).
[46] S. Bader Smoke, J. Magn. Magn. Mater. **100**(1–3), 440–454 (1991).
[47] Z. Tian, D. Sander, and J. Kirschner, Phys. Rev. B **79**(2), 024432 (2009).
[48] S. W. Sun and R. C. O'Handley, Phys. Rev. Lett. **66**(21), 2798–2801 (1991).
[49] R. O'Handley, O. S. Song, and C. Ballentine, J. Appl. Phys. **74**, 6302–6307 (1993).
[50] R. C. O'Handley and S. W. Sun, J. Magn. Magn. Mater. **104–107** (Part 3), 1717–1720 (1992).
[51] G. Wedler, J. Walz, A. Greuer, and R. Koch, Phys. Rev. B **60**(16), R11313–R11316 (1999).
[52] O. Hjortstam, K. Baberschke, J. M. Wills, B. Johansson, and O. Eriksson, Phys. Rev. B **55**(22), 15026–15032 (1997).
[53] G. Y. Guo, J. Magn. Magn. Mater. **209**(1–3), 33–36 (2000).
[54] K. Heinz, Rep. Prog. Phys. **58**(6), 637–704 (1995).
[55] O. Lysenko, V. Stepanyuk, W. Hergert, and J. Kirschner, Phys. Rev. Lett. **89**, 126102 (2002).
[56] O. Mironets, H. L. Meyerheim, C. Tusche, V. S. Stepanyuk, E. Soyka, P. Zschack, H. Hong, N. Jeutter, R. Felici, and J. Kirschner, Phys. Rev. Lett. **100**(9), 096103 (2008).
[57] V. Stepanyuk, D. Tsivlin, D. Sander, W. Hergert, and J. Kirschner, Thin Solid Films **428**, 1–5 (2003).
[58] T. U. Schülli, G. Vastola, M. I. Richard, A. Malachias, G. Renaud, F. Uhlk, F. Montalenti, G. Chen, L. Miglio, F. Schäffler, and G. Bauer, Phys. Rev. Lett. **102**(2), 025502 (2009).
[59] R. Vollmer, T. Gutjahr-Löser, J. Kirschner, S. van Dijken, and B. Poelsema, Phys. Rev. B **60**, 6277–6280 (1999).
[60] M. V. Rastei, B. Heinrich, L. Limot, P. A. Ignatiev, V. S. Stepanyuk, P. Bruno, and J. P. Bucher, Phys. Rev. Lett. **99**(24), 246102 (2007).
[61] B. Schulz and K. Baberschke, Phys. Rev. B **50**(18), 13467–13471 (1994).
[62] S. Müller, B. Schulz, G. Kostka, M. Farle, K. Heinz, and K. Baberschke, Surf. Sci. **364**(3), 235–241 (1996).
[63] W. Platow, U. Bovensiepen, P. Poulopoulos, M. Farle, K. Baberschke, L. Hammer, S. Walter, S. Müller, and K. Heinz, Phys. Rev. B **59**(19), 12641–12646 (1999).
[64] C. Uiberacker, J. Zabloudil, P. Weinberger, L. Szunyogh, and C. Sommers, Phys. Rev. Lett. **82**, 1289–1292 (1999).
[65] F. Máca, A. Shick, J. Redinger, R. Podloucky, and P. Weinberger, Czech. J. Phys. **53**, 33–39 (2003).
[66] F. Máca, A. Shick, G. Schneider, and J. Redinger, J. Magn. Magn. Mater. **272–276**, 1194–1195 (2004).
[67] H. Oka, P. A. Ignatiev, S. Wedekind, G. Rodary, L. Niebergall, V. S. Stepanyuk, D. Sander, and J. Kirschner, Science **327**(5967), 843–846 (2010).
[68] D. Sander, S. Ouazi, V. Stepanyuk, D. Bazhanov, and J. Kirschner, Surf. Sci. **512**, 281–286 (2002).
[69] W. Pan, D. Sander, M. T. Lin, and J. Kirschner, Phys. Rev. B **68**(22), 224419 (2003).
[70] R. M. Wang, O. Dmitrieva, M. Farle, G. Dumpich, H. Q. Ye, H. Poppa, R. Kilaas, and C. Kisielowski, Phys. Rev. Lett. **100**(1), 017205 (2008).
[71] R. Wiesendanger, Rev. Mod. Phys. **81**(4), 1495–1550 (2009).
[72] L. Diekhöner, M. A. Schneider, A. N. Baranov, V. S. Stepanyuk, P. Bruno, and K. Kern, Phys. Rev. Lett. **90**(23), 236801 (2003).
[73] O. Pietzsch, S. Okatov, A. Kubetzka, M. Bode, S. Heinze, A. Lichtenstein, and R. Wiesendanger, Phys. Rev. Lett. **96**(23), 237203 (2006).
[74] P. Weinberger, Phys. Rev. B **81**(17), 174410 (2010).
[75] L. Gerhard, T. Yamada, T. Balashov, A. Takacs, R. Wesselink, M. Däne, M. Fechner, S. Ostanin, A. Ernst, I. Mertig, and W. Wulfhekel, Nature Nanomater. **5**(11), 792–797 (2010).
[76] K. Tao, V. S. Stepanyuk, W. Hergert, I. Rungger, S. Sanvito, and P. Bruno, Phys. Rev. Lett. **103**(5), 057202 (2009).
[77] P. Weinberger, Phys. Rev. B **81**(18), 184412 (2010).